Contrib Mineral Petrol (1996) 123: 223–237

Karsten M. Haase · Colin W. Devey · Dieter F. Mertz
Peter Stoffers · Dieter Garbe-Schönberg

Geochemistry of lavas from Mohns Ridge, Norwegian-Greenland Sea: implications for melting conditions and magma sources near Jan Mayen

Received: 3 May 1995 / Accepted: 6 November 1995

Abstract Mohns Ridge lavas between 71 and 72°30′N (~360 km) have heterogeneous compositions varying between alkali basalts and incompatible-element-depleted tholeiites. On a large scale there is a continuity of incompatible element and isotopic compositions between the alkali basalts from the island Jan Mayen and Mohns Ridge tholeiites. The variation in isotopes suggests a heterogeneous mantle which appears to be tapped preferentially by low degree melts (~5%) close to Jan Mayen but also shows its signature much further north on Mohns Ridge. Three lava types with different incompatible element compositions [e.g. chondrite-normalized $(La/Sm)_N$<1 to >2] occur in the area at 72°N and were generated from this heterogeneous mantle. The relatively depleted tholeiitic melts were mixed with a small degree melt from an enriched source. The elements Ba, Rb and K of the enriched melt were probably buffered in the mantle by residual amphibole or phlogopite. That such a residual phase is stable in this region of oceanic mantle suggests both high water contents and low mantle temperatures, at odds with a hotspot origin for Jan Mayen. Instead we suggest that the melting may be induced by the lowered solidus temperature of a "wet" mantle. Mohns MORB (mid ocean ridge basalt) and Jan Mayen area alkali basalts have high contents of Ba and Rb compared to other incompatible elements (e.g. Ba/La >10). These ratios reflect the signature of the mantle source. Ratios of Ce/Pb and Rb/Cs are normal MORB mantle ratios of 25 and 80, respectively, thus the enrichments of Ba and Rb are not indicative of a sedimentary component added to the mantle source but were probably generated by the influence of a metasomatizing fluid, as supported by the presence of hydrous phases during the petrogenesis of the alkali basalts. Geophysical and petrological models suggest that Jan Mayen is not the product of hotspot activity above a mantle plume, and suggest instead that it owes its existence to the unique juxtaposition of a continental fragment, a fracture zone and a spreading axis in this part of the North Atlantic.

K.M. Haase (✉)[1] · C.W. Devey · P. Stoffers
D. Garbe-Schönberg
Geologisch-Paläontologisches Institut der Universität Kiel,
Olshausenstr. 40, D-24118 Kiel, Germany

D.F. Mertz
Institut für Geowissenschaften der Universität,
D-55099 Mainz, Germany

[1] *Present address:*
Max-Planck-Institut für Chemie,
Postfach 3060, D-55020 Mainz, Germany

Editorial responsibility: J. Hoefs

Introduction

While the geophysical processes at oceanic spreading centres are relatively well understood (Ahern and Turcotte 1978; Phipps Morgan 1987) fine-scaled studies of on- and off-axis basalts have shown that they are geochemically much more variable than previously thought (Bougault et al. 1988; Dosso et al. 1991; Castillo and Batiza 1989; Shirey et al. 1987). The causes for the generation of ridge magmas more enriched than "normal" depleted MORB (mid ocean ridge basalt) is still debated and various processes have been proposed. Enrichments in incompatible elements can in many cases be explained by variations in the proportions of melts extracted from different depths in the melt zone (Galer and O'Nions 1986; Plank and Langmuir 1992). The variation in isotopic composition can be attributed either to melting of a small scale heterogeneous mantle (Zindler et al. 1984) or to the influence of an enriched mantle plume (Schilling et al. 1983; Dosso et al. 1991). It is still unclear how large the compositional range of "normal" MORB is.

There is also no consensus on how exactly a plume may be recognized i.e. whether only by geophysical or also by geochemical means. The best plume indicators are probably an age-progressive volcanic chain and a positive bathymetric and geoid anomaly (Sleep 1990). Recent high-resolution seismic tomography studies have given the first indications of low velocity regions (=hot

mantle ± melt?) associated with some suspected plumes like Iceland or Gough/Tristan da Cunha (Zhang and Tanimoto 1993). Several authors have taken to suggesting incipient plume influx wherever MORB with a relatively enriched signature (e.g. $^{87}Sr/^{86}Sr > 0.703$, chondrite normalized $(La/Sm)_N > 1$) appears, although there may be no accompanying geophysical signature (Schilling et al. 1983; Dosso et al. 1991).

The Norwegian–Greenland Sea is one of the best-studied areas of the Earth's oceans and many bathymetric, geophysical and geochemical data exist for this region. Nevertheless, questions such as the origin of the volcanic island Jan Mayen and its surrounding seafloor have still not been convincingly answered. It has been suggested that the island sits above a mantle plume (Morgan 1981; Schilling et al. 1983). The lack of geophysical evidence for a plume has led other authors to doubt this hypothesis, and they have suggested the combination of a southwards propagating rift from the Mohns Ridge north of the Western Jan Mayen Fracture Zone (WJMFZ) with the proximity of the fracture zone as being the reason for the volcanism (Sylvester 1975; Imsland 1980; Saemundsson 1986).

In this study we investigate the chemistry of MORB from a restricted area on the Mohns Ridge in order to understand the melting processes and the distribution of the sources involved. We discuss the origin of the volcanism around Jan Mayen and compare it to the neighbouring spreading axes. We also review the evidence for and against a Jan Mayen plume.

Geological setting

North of the Western Jan Mayen Fracture Zone (WJMFZ), a small topographic ridge parallels the fracture zone which develops into an approximately 60 km wide bank opposite the island Jan Mayen (Fig. 1), the so-called Jan Mayen Platform (Neumann and Schilling 1984). The Jan Mayen Platform was probably generated at a northwards propagating spreading axis (Haase and Devey 1994). This Platform spreading centre has a strike parallel to Kolbeinsey Ridge, while Mohns Ridge north of about 71°30′N strikes in a more easterly direction. The spreading direction on the Platform spreading centre is parallel to the WJMFZ, i.e. WNW–ESE as indicated by fault plane solutions (Havskov and Atakan 1991). Fault plane solutions on Mohns Ridge north of 72°N suggest a more northerly plate movement approximately paralleling the Greenland Fracture Zone (Savostin and Karasik 1981; Havskov and Atakan 1991). This contradicts the model of Dauteuil and Brun (1993) who proposed a simple E–W spreading of Mohns Ridge based on structural observations.

The spreading axis directly north of the WJMFZ has a depth of about 1000 m, increasing northwards along Platform, Mohns and Knipovich Ridges to more than 2500 m at 72°N. Northern Mohns and Knipovich Ridges thus reach depths comparable to the global average axial depth of 2500 m of Parsons and Sclater (1977). Platform Ridge has an average depth of 1000 m and Mohns Ridge of approximately 2000 m (Fig. 1). The bulge of the Iceland Plateau is probably generated by the large Iceland mantle plume (Bott 1985). Although there may be a dynamic uplift or heat influence by the Iceland plume, no geochemical influence of the plume north of Iceland has been observed (Mertz et al. 1991).

The region south of the WJMFZ is dominated by the volcanic island Jan Mayen, situated on the anomalously shallow Jan Mayen Bank (<500 m deep, Fig. 1). South of the island, geophysical data suggest the existence of a continental fragment, the so-called Jan Mayen Ridge (Fig. 1, Myhre et al. 1984; Skogseid and Eldholm 1987), while there is no evidence for continental rocks underlying the Jan Mayen volcanoes themselves. The continental fragment formed a part of the Greenland margin at the onset of spreading 55 Ma ago and is covered in the east by sequences of seaward dipping reflectors, i.e. possible volcanics erupted at 55 Ma (Skogseid and Eldholm 1987). With the northward propagation of the Kolbeinsey Ridge some 43 Ma ago the fragment was split from the Greenland margin and drifted to its present position (Nunns 1982).

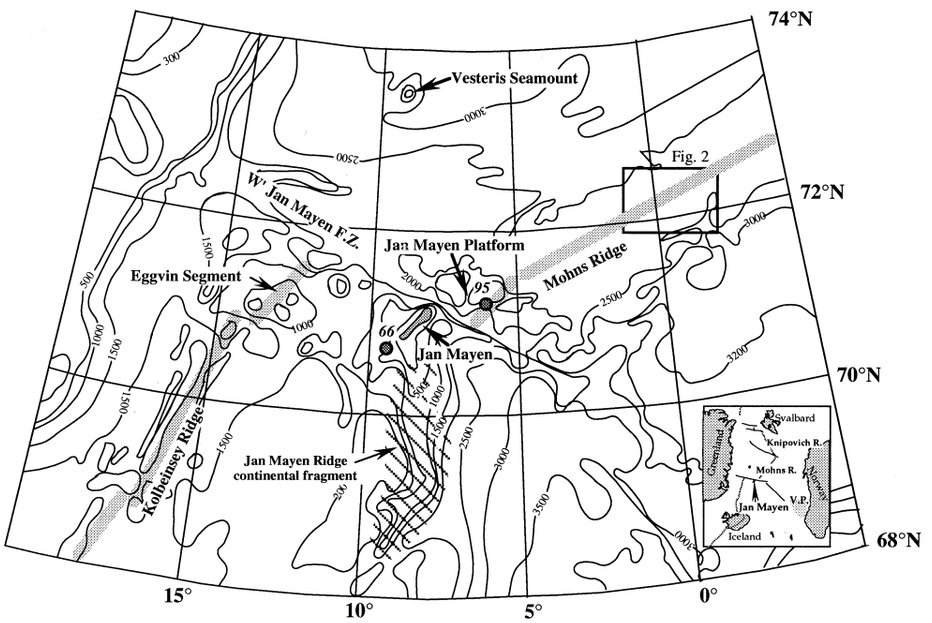

Fig. 1 Bathymetric map of the Norwegian–Greenland Sea redrawn after Perry (1985) with some isobaths and the most important structures. The *two dots* denote the sample stations 66 and 95. The *square* shows the position of the Mohns Ridge samples plotted in Fig. 2

Table 1 Locations of dredge and sediment corer stations

Number	Start Latitude	Longitude	End Latitude	Longitude	Depth range
21866 Jan Mayen Bank	70°30.50′N	8°53.35′W	70°30.86′N	8°52.72′W	542–464 m
23275 Mohns Ridge	71°57.14′N	0°42.46′W	71°58.20′N	0°43.76′W	2671–2355 m
23276-1 Mohns Ridge	71°58.35′N	0°36.47′W	71°59.42′N	0°35.89′W	2684–2524 m
23277-1 Mohns Ridge	72°02.3′N	0°36.9′W			2697 m
23280 Mohns Ridge	72°04.87′N	0°17.20′W	72°05.89′N	0°18.21′W	3031–2640 m
23288 Mohns Ridge	72°22.48′N	1°39.98′E	72°22.26′N	1°38.44′E	2573–2401 m
23291-2 Mohns Ridge	72°23.7′N	1°30.1′E			3200 m
23292 Mohns Ridge	72°24.28′N	1°44.92′E	72°23.91′N	1°42.79′E	3080–2698 m
428TVG Mohns Ridge	72°24.5′N	1°40.9′E	72°24.4′N	1°42.0′E	2759–2200 m
23295 Platform Ridge	71°08.90′N	5°54.85′W	71°09.29′N	5°53.74′W	1879–1773 m

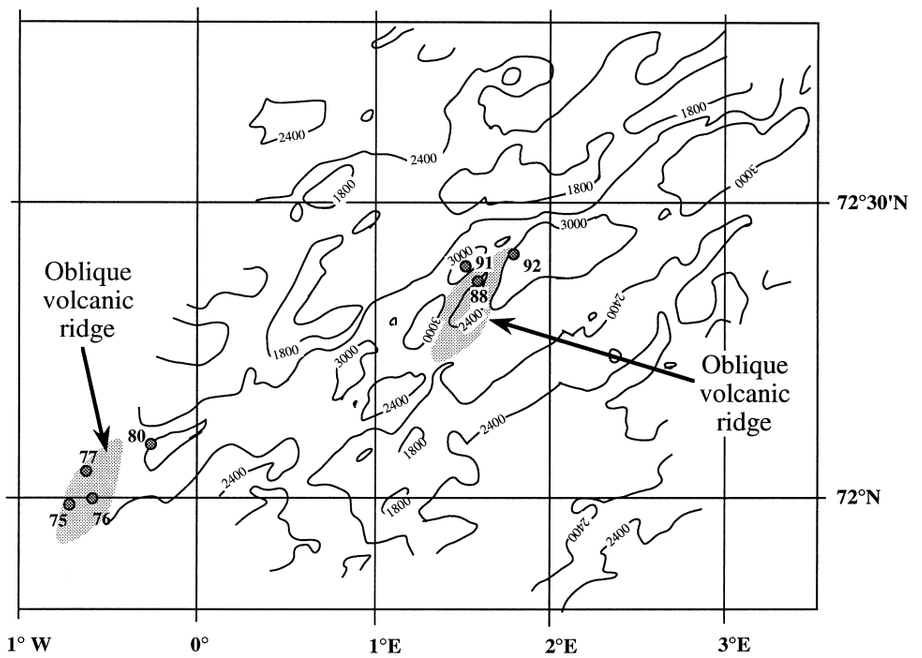

Fig. 2 Bathymetric map of a part of Mohns Ridge redrawn after Géli (1993). *Dots* mark the sample stations which come from two different ~500 m high oblique volcanic ridges within the en èchelon axial rift

Sampling and analytical methods

Sampling of the area was done during the cruise 7/3 of FS Meteor in 1988 (Mohns Ridge) and during the ARK VII/1 campaign of FS Polarstern in summer 1990 (Jan Mayen area). Sample locations are given in Table 1. In the text we will use the last two digits of the sample numbers for identification, e.g. 23291 reduces to 91. Most of the samples were obtained by dredging, although samples 91-2 and 77-1 are small pieces of basaltic glass from sediment box corers. The samples from the Mohns spreading axis come from a small area between 72 and 72°30′N where several samples were taken on two volcanic edifices which form en echelon structures along the axis (Fig. 2) (Géli 1993). The distance between these two sampling locations is about 90 km.

The samples were crushed and, where possible, glass was used for all analyses (denoted by "gl" behind the sample number). Glass was handpicked under a binocular microscope to obtain pieces with no visible signs of alteration. The crushed samples were washed several times to remove seawater and reduced to powder in an agate ball mill. The major elements were analysed with a Philips 1400 XRF (X-ray fluorescence) machine using international standards for calibration. Accuracy and precision can be seen in Table 3. The mineral analyses and some glass analyses of major elements were prepared using a Camebax microprobe at the Mineralogical Institute in Kiel. Constant Rb/Cs ratios of about 80 (Table 5) in the samples suggest that alteration, which might have affected the soluble elements, has not occurred.

Trace elements were analysed with a VG plasmaquad PQ-ICP-MS (inductively coupled plasma-mass spectrometry) at the Geo-

Table 2 Petrographic description of some representative samples with estimated volumes in vol.%. (*Ph* phenocrysts, *xeno* xenocrysts, *mph* microphenocrysts, *microlit* microlites, *variol* variolites)

Sample no.	Olivine	Plagioclase	Clinopyroxene	Matrix	Vesicles	Remarks
23275	<5% mph			Glass+microlit.	5%	
23276-1	5% mph	5% mph		Glass+microlit.	10%	
23288-3	Mph	Ph, xeno, mph		Glass+variol.	10%	
23292-1	1% ph+mph	30% ph+mph	1% xeno	Glass+microlit.	<5%	
23292-2	2% ph+mph	10% ph+mph		Glass+microlit.	20%	
23295-3	Ph	Ph	Ph	Tachylitic		
21866-A	3% ph	2% ph		Trachytic		
21866-B	1% ph	5% ph	3% ph	Tachylitic		Amphibole xeno
21866-E	7% ph	20% ph	3% ph	Intergranular	30%	
21866-G	20% ph	30% ph	1% mph	Tachylitic	5%	
21866-H	6% ph	4% ph	15% ph	Intergranular	40%	

Table 3 Major element analyses measured by XRF of basalts from the Mohns ridge and of the two international standards BIR and BHVO-1. 428TVG from Neubourg (1990). Alkaline basalts (AB) and trachybasalts (TB) from the Jan Mayen Bank. (CIPW norms and Mg # calculated assuming $FeO=0.85\ FeO^T$; *wr* whole rock, *gl* glass)

Sample	23275 wr	23276-2 wr	23277-1 gl	23280-4 wr	23288-2 wr	23288-3 wr	23291-2 gl	23292-1 wr	23292-2 wr	23295-3 wr	428TVG
SiO_2	50.06	49.99	50.68	49.75	49.33	50.67	52.07	49.13	50.04	49.73	52.10
TiO_2	1.115	1.063	1.268	1.084	1.138	1.150	1.050	0.760	1.137	1.823	1.72
Al_2O_3	15.24	15.61	14.96	15.25	15.08	15.47	15.14	20.59	15.29	15.55	14.59
$Fe_2O_3{}^T$	9.80	9.91	9.68	9.48	9.90	9.99	9.18	7.26	9.84	10.89	12.96
MnO	0.16	0.16	0.16	0.15	0.16	0.16	0.15	0.12	0.16	0.18	0.20
MgO	8.82	8.97	8.40	9.66	7.90	7.97	7.90	6.04	7.98	6.94	5.76
CaO	11.80	11.77	10.99	11.62	12.01	11.95	12.22	13.62	11.98	11.99	9.60
Na_2O	2.20	2.22	2.35	2.22	2.35	2.35	2.11	2.12	2.39	2.45	2.66
K_2O	0.309	0.295	0.547	0.330	0.333	0.320	0.240	0.090	0.306	0.820	0.66
P_2O_5	0.139	0.125	0.198	0.127	0.138	0.143	0.121	0.074	0.138	0.328	0.21
Sum	99.661	100.120	99.225	99.766	98.333	100.190	100.19	99.814	99.252	100.700	100.54
Mg #	67.74	67.86	66.93	70.39	65.05	65.05	66.75	65.99	65.92	59.78	50.90

Sample	21866-A	21866-B	21866-D	21866-E	21866-F	21866-G	21866-H	21866-I	BIR-1	BHVO-1	1σ
Rock type	AB	TB	AB	AB	AB	AB	TB	AB			(*n*=12)
SiO_2	46.25	47.79	46.86	46.19	45.10	46.92	46.55	46.97	47.31	49.71	0.16
TiO_2	2.88	2.85	3.14	3.07	2.86	2.00	3.26	2.93	0.98	2.797	0.016
Al_2O_3	14.56	16.54	15.61	16.58	14.18	10.31	16.32	15.36	15.47	13.66	0.05
$Fe_2O_3{}^T$	11.87	11.53	13.65	12.82	12.90	10.32	12.63	12.65	11.41	12.37	0.08
MnO	0.19	0.21	0.21	0.20	0.20	0.16	0.19	0.20	0.17	0.17	0.00
MgO	9.09	5.14	5.12	5.25	9.93	14.31	4.58	6.92	9.51	7.20	0.02
CaO	10.70	9.21	10.26	10.11	11.04	12.87	10.10	9.81	13.36	11.46	0.04
Na_2O	2.36	3.30	2.41	2.50	2.21	1.42	2.78	2.74	1.97	2.25	0.03
K_2O	1.53	1.97	2.11	2.39	1.08	1.36	2.56	2.09	0.030	0.522	0.003
P_2O_5	0.50	0.89	0.58	0.54	0.55	0.39	0.64	0.56	0.030	0.272	0.003
Sum	100.05	99.57	100.08	99.82	100.12	100.17	99.77	100.26	100.21	100.41	
Mg #	64.08	50.94	46.63	48.82	64.20	76.36	45.79	55.67			
CIPW norms											
Orthoclase	9.03	11.63	12.45	14.11	6.37	8.02	15.11	12.33			
Albite	16.97	26.33	20.37	16.56	15.62	9.15	17.20	19.16			
Anorthite	24.59	24.48	25.52	26.94	25.55	17.71	24.47	23.42			
Nepheline	1.61	0.85		2.48	1.66	1.54	3.41	2.17			
Diopside	20.40	12.65	17.86	16.23	20.73	34.82	17.74	17.65			
Hypersthene			0.16								
Olivine	17.40	12.51	12.12	12.36	19.50	20.98	10.16	14.70			
Magnetite	2.58	2.51	2.98	2.79	2.80	2.25	2.74	2.76			
Ilmenite	5.48	5.42	5.97	5.84	5.44	3.80	6.20	5.57			
Apatite	1.16	2.07	1.35	1.26	1.28	0.91	1.49	1.30			
Sum	98.92	98.45	98.79	98.56	98.95	99.18	98.53	99.06			

Table 4 Major element analyses of glasses measured by electron microprobe (ND not determined)

Sample	23275	23276-1	23288-2	23288-3	23292-1	23292-2	23295-3
SiO_2	51.03	50.62	50.80	51.33	51.41	51.50	50.48
TiO_2	1.11	1.10	1.11	1.06	1.15	1.07	1.94
Al_2O_3	15.11	16.49	14.82	15.01	14.52	14.52	14.29
FeO^T	8.66	8.44	8.52	8.45	9.21	9.55	10.04
MnO	0.15	0.17	0.14	0.14	0.17	0.18	0.17
MgO	8.05	8.12	7.95	7.97	7.70	7.53	6.13
CaO	12.15	11.93	11.88	11.76	12.48	11.50	11.03
Na_2O	2.21	2.12	2.38	2.63	2.32	2.53	2.17
K_2O	0.36	0.32	0.37	0.36	0.16	0.25	1.07
P_2O_5	ND	ND	ND	0.32	ND	0.28	ND
Sum	98.81	98.31	97.95	99.03	99.10	98.90	97.31
Mg #	66.11	66.89	66.21	66.44	63.70	62.34	56.17

logical Institute in Kiel after the method of Garbe-Schönberg (1993). Measurements of international standards which were run with the samples, and their long-term reproducibility, are given in Table 2.

Accuracy of the major element analyses generally is within (±)5% of the working values of Govindaraju (1994) recalculated on a volatile free basis, while the precision of our analyses is better than 2% (Table 3). Deviations from the working values of about 10% for Na_2O and K_2O and 50% for P_2O_5 occur for the low concentration elements in standard BIR-1. Most of our trace element data on standards lie within 10% of the working values of Govindaraju (1994) and the ID SSMS analyses of Jochum et al. (1990). Mean values of the international standards BIR-1 and BHVO-1 analysed together with the samples are shown in Table 5. The ICP-MS rare-earth elements and Y have in most cases slightly lower concentrations than in the other two data sets. Larger deviations of about 10% from the other analyses exist for Ba and Th in the depleted BIR-1, although Th is probably below the determination limit. The reproducibility is generally better than 5% for the trace elements with the exception of Cs and Th, which are 30% and 10%, respectively.

Results

Sample petrography is described in Table 2. Lavas from Mohns Ridge are mainly olivine and plagioclase phyric and in most cases the crystals are smaller than 2 mm. Only sample 92-1 shows plagioclase megacrysts (~30 vol.%, up to 10 mm) and a few strongly resorbed phenocrysts of clinopyroxene with composition $Wo_{44}En_{50}Fs_6$. The samples from the Jan Mayen Bank (dredge 66) contain abundant large phenocrysts of olivine, dark green Ti-augitic clinopyroxene and plagioclase. In sample 66-B, rounded phenocrysts of brown amphibole also occur. These Jan Mayen Bank samples are petrographically similar to the ankaramitic alkali basalts and trachybasalts of the island Jan Mayen as described by Imsland (1980). With the exception of the nepheline-normative sample 95-3 from the Jan Mayen Platform, all lavas recovered by us north of the WJMFZ are hypersthene normative and thus classified as tholeiites. Sample 95-3 resembles the lavas from the Jan Mayen Bank (66) and Jan Mayen petrographically and geochemically (Tables 2 and 3). Signs of alteration were not observed in the MORB glasses, while some of the alkaline lavas from the Jan Mayen Bank contain thin coatings of alteration phases in the vesicles.

On Fig. 3 major and minor elements of the tholeiitic Mohns Ridge MORB are plotted against MgO and compared to previously published data from the Mohns Ridge and Jan Mayen Platform and Kolbeinsey Ridge. Our data fit well with the published data on Mohns lavas, but sample 428TVG plots at a lower MgO content. The Mohns tholeiites generally have SiO_2 contents above 50% which is higher than for Kolbeinsey lavas at a given MgO value. Mohns Ridge MORB have lower CaO than the primitive Kolbeinsey lavas and it appears that they follow two distinct fractionation trends in CaO with increasing CaO between 9.5 and 7.5% MgO (Fig. 3). Sample 80-4 is the most primitive of the high-CaO trend, sample 77-1 is a primitive member of the low-CaO trend. Kolbeinsey MORB follow a typical tholeiitic trend of FeO^T (total iron as FeO) enrichment, in contrast the Mohns lavas show relatively constant FeO^T between 10 and 7% MgO. Mohns MORB with more than 7% MgO have higher TiO_2 and Na_2O than Kolbeinsey lavas at a given MgO content. In the diagram of K_2O versus MgO, basalts from the Mohns and Jan Mayen Platform spreading axis show a wide variation from low-K tholeiites to alkali basalts with K_2O of about 1% and cluster around 0.3 and 0.5%. Sample 91-2 belongs to the low-K tholeiite group while 80-4 is intermediate and 77-1 has a high K_2O content of about 0.5%.

Figure 4 confirms that, with respect to the rare-earth elements, three different MORB types occur in the study area around 72°N, and lavas with various La/Sm are present in one dredge (e.g. dredge 92). Most of the Mohns samples show enrichment in light rare-earth elements ($La/Sm_N>1$). The most primitive tholeiite 80-4 belongs to this main group with a $(La/Sm)_N$ of about 1.3, while the most enriched lava 77-1 has a $(La/Sm)_N$ of 2.17. Only lava 92-1 is light rare-earth element depleted and is one of the tholeiites with the lowest incompatible element contents in the published Mohns MORB suite. The alkali basalt of the Jan Mayen Platform (Fig. 4) has high enrichments of light rare earths with $(La/Sm)_N$ above 3 which is similar to the Jan Mayen alkali basalts.

Table 5 Trace element concentrations (in ppm) of Mohns Ridge MORB and alkali basalts from Jan Mayen Bank (21866). Also given are means of analyses of the standards BIR-1 and BHVO-1 run with the samples and the 1σ standard deviations of BHVO-1

Sample	23275wr	23276-2	23277-1	23280-4	23288-2	23288-3	23291-2	23292-1	23292-2	428TVG	23295-3	21866-D	21866-F	21866-G	BIR-1	BHVO-1	SD (n=11)
Sc	38.5	36.7	37.0	33.5	40.3	38.7	36.3	26.0	37.3	41.8	35.9	24.4	31.9	38.0	39.9	31.4	3.2
Cr	366	389	385	483	178	173	395	231	173	14.7	93.5	17.6	541	1043	445	312	28
Co	46.6	45.3	45.5	44.2	47.9	45.0	42.1	32.9	44.2	43.8	47.8	48.4	55.7	57.7	54.2	44.6	2.4
Ni	149	156	150	180	96.1	91.3	99.4	82.9	91.3	22.9	48.2	38.1	167	278	172	118	6
Cu	89.9	89.5	87.2	78.4	92.3	86.4	85.5	62.6	87.4	56.3	57.1	98.3	88.2	104	120	140	13
Zn	72.6	71.4	74.7	66.6	75.2	74.1	65.7	54.5	76.1	93.7	85.1						
Y	23.4	23.4	25.0	22.6	25.0	24.9	22.0	17.3	24.8	31.6	24.4	21.5	22.3	13.8	14.9	25.7	0.8
Rb	8.51	7.36	14.3	7.12	8.04	7.69	6.19	2.20	7.79	13.2	18.0	48.8	22.7	31.1	0.23	9.29	0.78
Cs	0.11	0.09	0.19	0.12	0.10	0.09	0.07	0.03	0.08	0.15	0.19	0.60	0.25	0.33	0.010	0.10	0.05
Sr	132	120	185	117	128	126	113	104	127	146	348	653	612	418	98.7	372	31
Ba	94.8	81.4	167	80.7	98.0	95.6	74.6	28.7	97.7	175	305	759	367	465	9.84	122	7
Zr	64.5	57.7	84.5	58.3	61.0	61.3	53.2	34.4	61.8	102	127	199	188	126	12.9	171	9
Hf	1.68	1.44	2.13	1.73	1.76	1.70	1.49	1.09	1.76	3.22	3.14	4.34	4.41	2.99	0.51	4.08	0.42
Nb	8.36	6.22	15.8	7.25	8.31	7.98	5.71	1.76	7.80	17.6	40.4	81.7	47.8	54.2	0.71	17.8	1.5
Pb	0.60	0.43	0.92	0.50	0.55	0.53	0.47	0.27	0.55	1.05	1.24	3.19	1.83	1.61	2.71	1.99	0.157
Th	0.60	0.44	1.12	0.53	0.52	0.54	0.38	0.11	0.53	1.06	2.30	4.32	2.63	2.88	0.03	1.08	0.09
U	0.20	0.14	0.36	0.18	0.21	0.21	0.12	0.04	0.18	0.28	0.83	1.87	0.96	0.93	0.01	0.42	0.02
La	6.36	4.83	11.0	5.30	5.74	5.71	4.25	1.89	5.73	10.5	25.2	43.7	30.6	30.1	0.57	14.3	0.7
Ce	14.6	11.6	23.4	12.4	13.4	13.4	10.4	5.50	13.5	24.2	52.8	89.1	66.8	60.7	1.82	36.3	1.6
Pr	2.03	1.70	2.99	1.79	1.89	1.87	1.53	0.90	1.91	3.45	6.29	10.5	8.51	7.06	0.35	5.09	0.28
Nd	9.48	8.14	12.9	8.47	8.88	8.96	7.48	4.86	9.11	15.5	24.8	39.6	35.0	26.8	2.23	23.4	1.3
Sm	2.74	2.50	3.27	2.55	2.60	2.58	2.34	1.69	2.62	4.60	5.07	7.00	7.05	4.69	1.05	5.94	0.45
Eu	0.94	0.90	1.11	0.93	0.96	0.94	0.85	0.66	0.96	1.51	1.58	2.15	2.24	1.45	0.48	1.95	0.07
Gd	3.30	3.10	3.75	3.11	3.28	3.26	2.88	2.14	3.24	5.24	4.98	5.81	6.08	3.87	1.62	6.00	0.30
Tb	0.57	0.56	0.62	0.57	0.56	0.57	0.50	0.40	0.58	0.95	0.70	0.82	0.86	0.54	0.32	0.87	0.07
Dy	3.67	3.61	4.00	3.67	3.79	3.85	3.43	2.71	3.86	5.96	4.07	4.41	4.70	2.90	2.27	4.95	0.40
Ho	0.77	0.78	0.82	0.77	0.79	0.80	0.72	0.57	0.81	1.35	0.79	0.80	0.85	0.53	0.50	0.89	0.07
Er	2.31	2.34	2.44	2.27	2.35	2.38	2.13	1.71	2.44	3.85	2.25	2.22	2.30	1.42	1.48	2.25	0.13
Tm	0.34	0.34	0.35	0.33	0.34	0.35	0.31	0.5	0.35	0.55	0.32	0.29	0.30	0.19	0.21	0.30	0.02
Yb	2.13	2.18	2.28	2.15	2.32	2.36	2.13	1.64	2.32	3.75	2.06	1.90	1.92	1.17	1.47	1.89	0.14
Lu	0.33	0.33	0.33	0.32	0.33	0.33	0.30	0.24	0.34	0.54	0.30	0.25	0.26	0.16	0.21	0.25	0.02
$(La/Sm)_N$	1.50	1.25	2.17	1.34	1.42	1.43	1.17	0.72	1.41	1.47	3.21	4.03	2.80	4.14			
Ba/La	14.9	16.9	15.2	15.2	17.1	16.7	17.6	15.2	17.1	16.7	12.1	17.4	12.0	15.4			
Rb/Cs	77.4	81.8	75.3	59.3	80.4	85.4	88.4	73.3	97.4	88.0	94.7	81.3	90.8	94.8			
Ce/Pb	24.5	26.8	25.4	24.8	24.5	25.2	22.2	20.7	24.4	23.0	42.6	27.9	36.5	37.7			

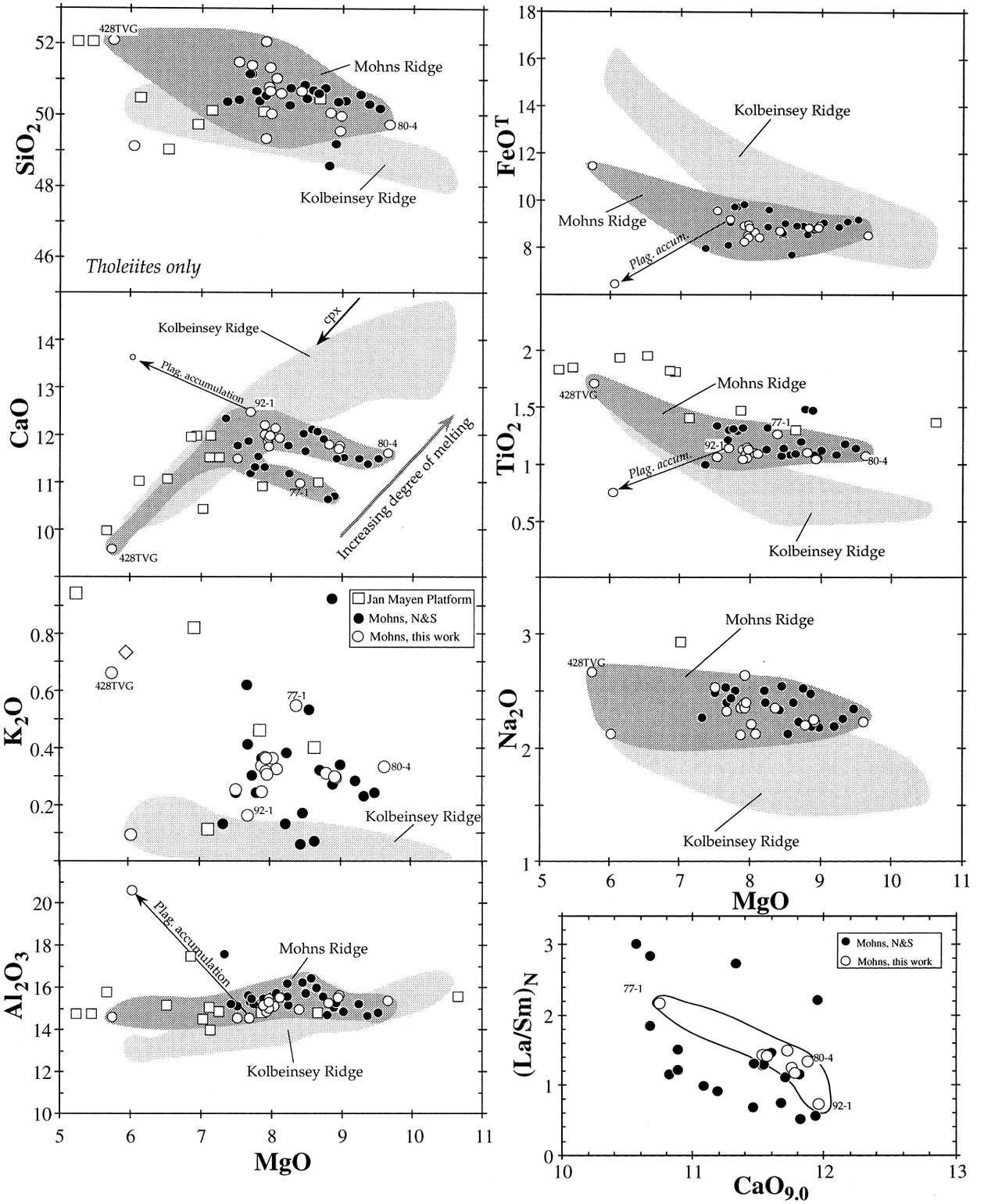

Fig. 3 SiO_2, CaO, K_2O, FeO^T (total iron as FeO), TiO_2, and Na_2O and MgO for tholeiites from the spreading axes of Mohns and Kolbeinsey Ridges and from the Jan Mayen Platform. Note the two different trends for CaO versus MgO which are outlined by the *fields*. The *arrows* on the plots of FeO^T, CaO, Al_2O_3 and TiO_2 show the effect of plagioclase accumulation between the glass and the whole rock 23292-1. *Open circles* are data from this paper. Data from Schilling et al. (1983), Neumann and Schilling (1984), Maaløe et al. (1986), Devey et al. (1994)

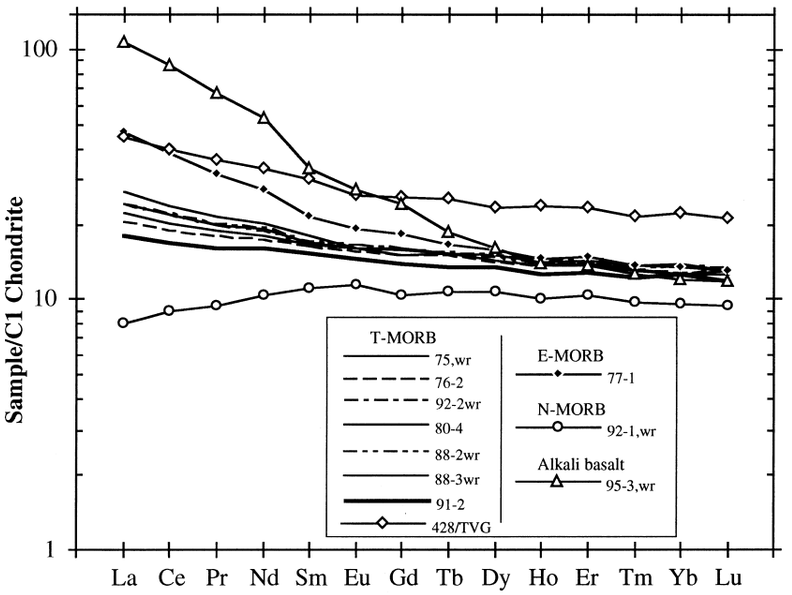

Fig. 4 Rare-earth element plot of the Mohns Ridge samples normalized to chondrite from Sun and McDonough (1989). The tholeiites are classified according to their light-rare-earth element enrichments into N-, T-, and E-MORB. Note that 95-3 is an alkali basalt from the Jan Mayen Platform

Discussion

Major element fractionation

In the following we will concentrate on the generation of the Mohns Ridge tholeiites because the petrogenesis of the alkali basalts in the Jan Mayen area has already been extensively studied (Imsland 1980; Neumann and Schilling 1984; Maaløe et al. 1986). Sigurdsson (1981) divided North Atlantic MORB into two groups and showed that Mohns Ridge lavas resemble MORB between 35 to 53°N in having high SiO_2, Na_2O and K_2O but low FeO^T compared to MORB between 54 and 70°N. These major element differences have been attributed either to clinopyroxene fractionation at depth (Sigurdsson 1981; Neumann and Schilling 1984) or to source heterogeneity (Klein and Langmuir 1987).

Olivine dominates the fractionation assemblage between 9.5 and 8% MgO in Mohns MORB, leading to shallow trends for most elements when plotted against MgO (Fig. 3). The onset of clinopyroxene fractionation may be indicated by strongly decreasing CaO and appears at about 7% MgO in the low-CaO group compared to about 8% MgO for the high-CaO group and even higher MgO in the Kolbeinsey suite (Fig. 3). In our samples, clinopyroxene only occurs as corroded megacrysts in one sample (92-1, 7.7% MgO) suggesting that it is generally not in equilibrium with Mohns tholeiites. Thus we reject the idea of Sigurdsson (1981) that clinopyroxene occurs throughout the compositional range of Mohns MORB. The difference between the high-CaO and the low-CaO versus MgO trend appears to correspond to the differences in the incompatible element contents of the lavas, as 77-1 with low CaO has high TiO_2 and K_2O while the primitive high-CaO lava 80-4 has lower TiO_2 and K_2O concentrations. There is a broad negative correlation between fractionation-corrected CaO and La/Sm in the Mohns data set (Fig. 3). Thus, we would also rule out the differences between the high- and low-CaO groups as being due to clinopyroxene resorption, as this phase does not affect the K_2O content or $(La/Sm)_N$ ratio strongly. The large range of CaO in the primitive Mohns tholeiites combined with the changes in the incompatible element compositions suggest that processes other than crystal fractionation also play a role in the petrogenesis. As CaO is compatible in the mantle, its concentration in a melt will be more sensitive to variations in the degree of partial melting than to mantle heterogeneity.

Figure 3 shows that primitive Mohns tholeiites have higher Na_2O contents than Kolbeinsey MORB at the same MgO contents. The averages of $Na_{8.0}$ in Norwegian–Greenland Sea MORB rise from 1.98 ± 0.22 for Kolbeinsey Ridge and 2.14 ± 0.28 for Eggvin to 2.35 ± 0.12 on Mohns and 2.80 ± 0.15 on Knipovich Ridges (calculated as $Na_{8.0} = Na_2O + 0.06\ MgO - 0.48$ for Mohns and Knipovich lavas with more than 6% MgO). Following the reasoning of Klein and Langmuir (1987), this implies a northerly decreasing degree of partial melting assuming that Na_2O is homogeneously distributed in the mantle. From experimental data, Kinzler and Grove (1992) calculated major element compositions of accumulated melts generated by an upwelling mantle column. Their results are plotted in Fig. 5 together with the MORB compositions of the Norwegian–Greenland Sea spreading centres. The lavas from the three spreading axes fall into different groups, suggesting the lowest degree of melting for Knipovich and the highest degree of melting for Kolbeinsey MORB. Mohns tholeiites are in the range of 12 to 13% accumulated melt and follow a steep trend to higher Na_2O with increasing FeO^T. Thus the Na_2O contents of Mohns MORB do not support the idea of large variations in the degrees of partial melting, which might be inferred from the CaO concentrations.

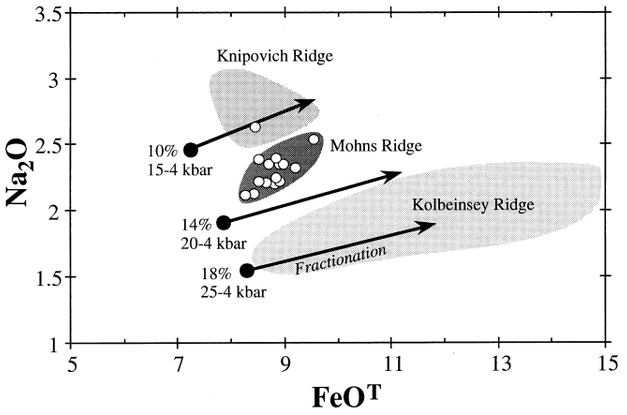

Fig. 5 Plot of Na_2O versus FeO^T after Kinzler and Grove (1992). Mohns MORB data are only from this paper. The *filled circles* mark accumulated melt compositions at 10, 14 and 18% melting. *Arrows* denote 50 to 60 wt% crystal fractionation at high pressure after Kinzler and Grove (1992). *Numbers with kbars* give the calculated pressure range of melting. Data sources as in Fig. 3

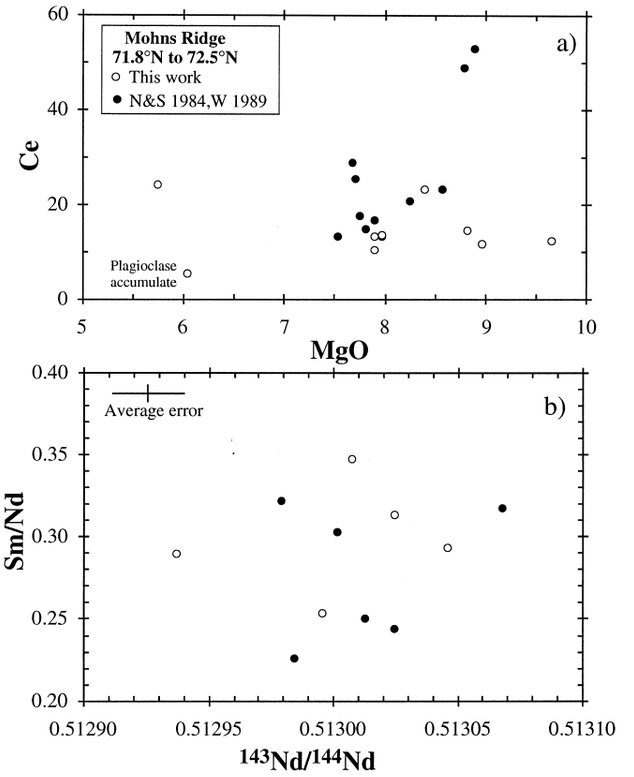

Fig. 6a Ce versus MgO and **b** Sm/Nd versus $^{143}Nd/^{144}Nd$ for samples from the study area between 71.8°N and 72.5°N on Mohns Ridge. The Nd isotopes are recalculated to values of BCR-1: 0.512633 and LaJolla: 0.511855. *Filled circles* are data from Neumann and Schilling (1984) and Waggoner (1989), *open circles* Nd isotopes from Mertz, DF, Raczek, I, Devey, CW (unpublished)

However, the effect of H_2O on the Na_2O contents of melts is only poorly understood for water-undersaturated systems although it appears that FeO^T is relatively unaffected by variable H_2O contents (Hirose and Kawamoto 1995). Note that although the involvement of water may have large effects on the fractionating phases (Michael and Chase 1987) this will not affect our $CaO_{9.0}$ calculations as they were calculated based on the actual trends in Fig. 3.

Trace element fractionation

The Mohns Ridge lavas between 71.8 and 72.5°N have variable incompatible element compositions with Ce ranging between about 10 and 50 ppm at MgO contents of 8 to 9% (Fig. 6a). The range in $^{143}Nd/^{144}Nd$ of the samples at 72°N is limited to 0.51293 to 0.51307. Sm/Nd ranges between 0.22 and 0.35 in this narrow range of $^{143}Nd/^{144}Nd$ but no correlation is observed. This implies that the lavas at 72°N on Mohns Ridge are derived from slightly variable sources but that probably the main effect of enrichment and Sm/Nd fractionation is due to recent (i.e. melting) processes, allowing no time for changes in Nd isotope compositions to occur.

Figure 7 shows depleted MORB-normalized concentrations of representative lavas. Although the concentrations vary by a factor of ~10, the similarities in the basic shape of the incompatible element patterns of all tholeiites from the Jan Mayen area suggest that they reflect the signature of the mantle source. The patterns of these samples differ significantly from the smooth pattern of average enriched MORB (Fig. 7). The alkali basalt from the Jan Mayen Platform (95-3) shows a distinct pattern with a marked peak at Ba but decreasing Rb and Cs. Variable degrees of partial melting lead to some rotation of the patterns of the tholeiites, but is not responsible for the peaks and troughs seen. All tholeiitic basalts have strong relative enrichments of Cs, Rb, Ba, K, and to a lesser extent Pb and Sr compared to the other incompatibles. The preferential enrichments of these elements cannot be explained by the influence of any known melt (e.g. Green 1994) but they are known to be strongly soluble in hydrous fluids (Tatsumi et al. 1986). The observed anomalous enrichments of these elements in many subduction-related lavas (e.g. back-arc basalts, Fig. 7) is thought to be the result of an influx of fluids into the mantle source (Tatsumi et al. 1986; Woodhead 1989). Schilling et al. (1980) noted a strong positive correlation between Ba, Rb, and K enrichment and Br and Cl contents in MORB near the Azores and suggested a mantle enrichment by halogen-rich fluids. Thus, we suggest that either hydrous and/or Cl-Br-rich fluids probably led to the enrichment of the sources of the Jan–Mayen–Mohns Ridge region tholeiites and, possibly, alkali basalts. However, slight differences in the source compositions exist and the higher Sr and lower Nd isotopic ratios of the alkali basalts point to different Rb/Sr and Sm/Nd ratios in their sources (Waggoner 1989).

Subduction zone lavas also show strong enrichment of U and depletions in Nb, which are not seen in the basalts

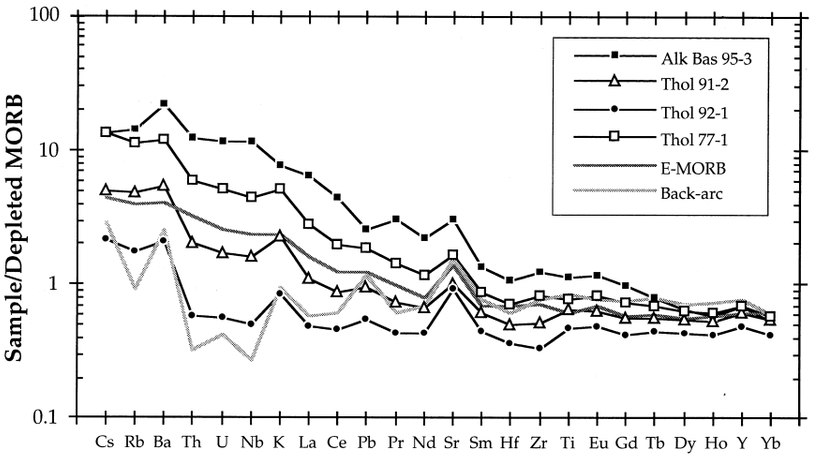

Fig. 7 Depleted-MORB-normalized diagram for representative samples with MORB values from Hofmann (1988). Data for Lau backarc basin basalt from Hergt and Farley (1994) and for average enriched MORB from Sun and McDonough (1989)

of this study. The solubility of U depends on its oxidation state, under reducing conditions (U^{4+}) it is less soluble than as U^{6+}. Ballhaus (1993) has shown that enriched MORB have generally higher oxidation states than depleted MORB but are still lower than subduction-related basalts. Because the oceanic mantle has a lower f_{O_2} than the mantle in subduction zones, U may show a different behaviour underneath the Mohns Ridge and Jan Mayen region despite an enrichment in volatiles relative to normal MORB mantle. The Nb depletion in subduction-related magmas is thought to be the result either of the presence of a high-field-strength element-bearing residual phase during melting or of the selective addition of large-ion-lithophile and rare-earth elements to the mantle source (see Hawkesworth et al. 1993 for review). If this Nb depletion is generated during the melting process beneath magmatic arcs, its absence in the North Atlantic samples simply reflects the fact that the Mohns Ridge is not a subduction zone and so has different *P–T*-volatile conditions at melting. It is possible, for example, that the volatile-bearing mantle phase is different, and that rather than being the Nb-buffering phase amphibole (as suggested for arcs by several authors, e.g. McKenzie and O'Nions 1991) in the mantle beneath the study area it might be phlogopite (which has high $D^{Rb/Ba}$ of ~ 2 but relatively low $D^{Nb/La}$, Adam et al. 1993; Ionov and Hofmann 1995). If, on the other hand, the Nb-depletion in arcs is due to selective addition of some elements, it did not carry as many elements in the sub-oceanic regime as at a subduction zone.

In the Mohns Ridge area, the occurrence, over a limited area, of MORB and alkali basalts with some geochemical overlap (e.g. Sr-Nd isotopes, incompatible element patterns) led Waggoner (1989) to propose the mixing of the enriched Jan Mayen magmas with depleted MORB. In Fig. 8 we test this hypothesis. The model of melt mixing can account for the trends of $(Ce/Yb)_N$ versus $(Tb/Yb)_N$ and $^{143}Nd/^{144}Nd$ for all Mohns Ridge MORB (Fig. 8). Most lavas plot close to the mixing lines between a MORB melt formed by 10% melting in the spinel lherzolite field and a melt having the isotopic composition of Jan Mayen area alkali basalts and formed from an enriched source at 5% melt with garnet as the stable Al-phase.

A difference exists between the Jan Mayen alkali basalts and the tholeiites with the former having relatively low concentrations in Rb and K compared to Ba or Th. This difference can be observed in Fig. 9, where the Mohns tholeiites show lower Ba/Rb than the alkali basalts and a negative correlation between Rb/Th and Th. The tholeiitic trend in Rb/Th points towards the alkali basalt field, implying a transition in the petrogenetic conditions from the tholeiitic to the alkaline lavas. This trend can be either a mixing trend or it suggests that for the alkali basalt genesis Rb was more compatible than Th. We do not think that mixing is responsible, as the high Rb/Th tholeiites from the Mohns Ridge are isotopically less radiogenic than the alkali basalts (Fig. 10), implying that the tholeiite source has a time-integrated depletion in, for example, Rb. That the relatively Rb rich alkali basalt source produces basalts with higher Ba/Rb implies that a residual phase is making Rb more compatible than Ba during melting. The only abundant phases known to have a buffering effect on Ba and Rb (and K, not shown) in the mantle are the hydrous phases phlogopite or amphibole (Sun and McDonough 1989). Unfortunately it is not clear whether these hydrous phases are stable at the high temperatures of the oceanic mantle (Mengel and Green 1989; Sudo and Tatsumi 1990). Recent experiments of Adam et al. (1993) suggest temperatures of less than 1100° C at 10 to 20 kbar where amphibole or mica are stable in the presence of a melt. This may imply either low temperatures underneath Mohns Ridge or another buffering phase.

Mantle sources

Enriched mantle sources may be generated by two processes which are (1) recycling of crustal or old continental lithospheric material, (2) metasomatism in the mantle (e.g. Sun and McDonough 1989). For the enriched

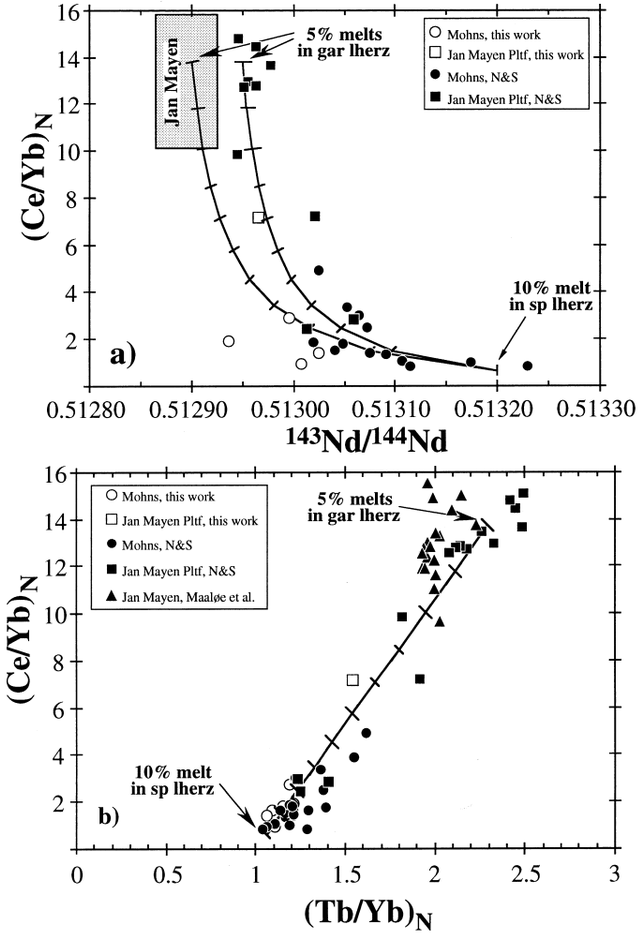

Fig. 8a $(Ce/Yb)_N$ versus $^{143}Nd/^{144}Nd$ and two mixing lines between a 10% MORB melt from spinel lherzolite and two 5% melts generated in garnet lherzolite with different isotopic compositions. **b** $(Ce/Yb)_N$ versus $(Tb/Yb)_N$ and a mixing line between a 10% MORB melt from spinel lherzolite and a 5% melt generated in enriched garnet lherzolite. Each *tick mark* is for 10% mixing. Data sources: distribution coefficients and MORB source McKenzie and O'Nions (1991); enriched source: amphibole lherzolite Z-35, Bonatti et al. (1986) with 0.1 ppm Tb. Mantle mineralogy: MORB o165opx20cpx10sp5, enriched mantle o160opx25cpx10gar5. Melting modes from Gudfinnson and Presnall (1993) for 24 kbar (MORB) and 34 kbar (enriched mantle). Batch melting model of Shaw (1970). Other data sources as in Fig. 3 and Nd isotopes from Mertz et al. (unpublished)

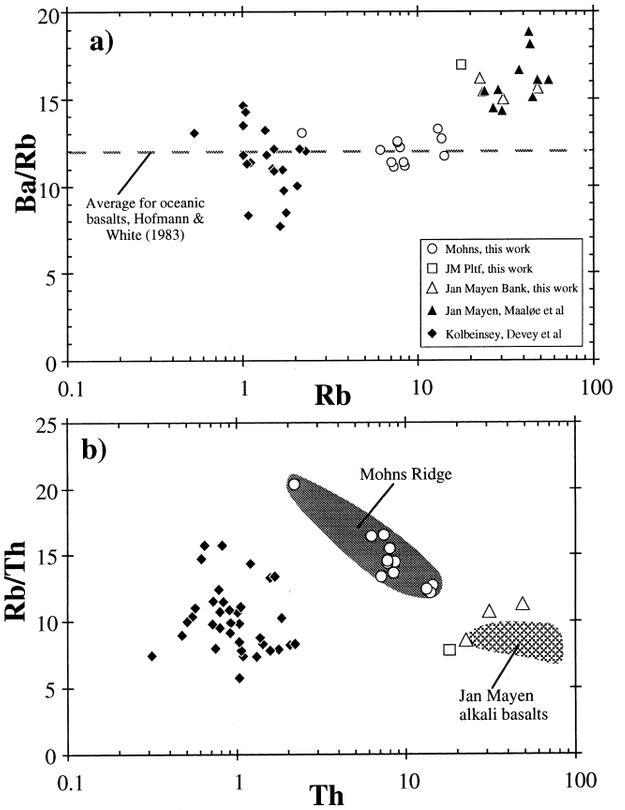

Fig. 9 **a** Ba/Rb versus Rb and **b** Rb/Th versus Th for Mohns and Kolbeinsey MORB and Jan Mayen area alkali basalts. Average of global oceanic volcanics after Hofmann and White (1983). Data sources as in Fig. 3

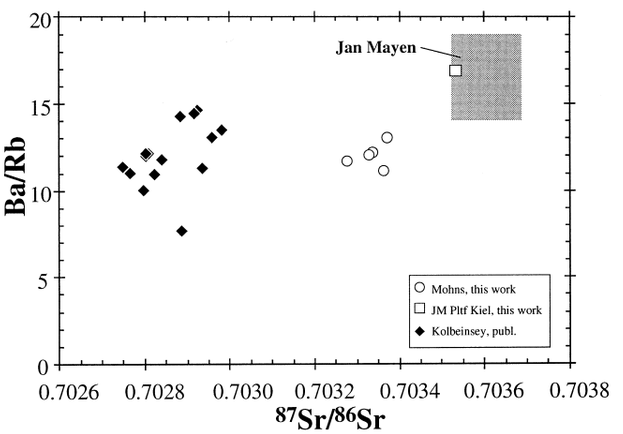

Fig. 10 Ba/Rb versus $^{87}Sr/^{86}Sr$ showing a positive correlation for lavas from the Jan Mayen/Mohns Ridge lavas. Isotopes for our samples are from Mertz et al. (unpublished). Data sources: Devey et al. (1994), Maaløe et al. (1986), Mertz et al. (1991), O'Nions and Pankhurst (1974)

mantle of Jan Mayen, Kurz et al. (1982) proposed a MORB source with a recycled sediment component similar to that of Gough/Tristan da Cunha on the basis of the low $^3He/^4He$ (6.5 R/Ra) ratios. Waggoner (1989) suggested a model in which a basanitic (<0.1%) melt from recycled oceanic crust metasomatized a mantle portion at a subduction zone 450 Ma ago. This mantle portion was subducted and after several hundred Ma ascended as a mantle plume at Jan Mayen.

High Ba/La in Jan Mayen and Mohns Ridge magmas would seem to support the model of recycled oceanic crust with sediment in the Norwegian–Greenland Sea mantle because sediments have high Ba/La (Fig. 11). In altered oceanic crust the $^{87}Sr/^{86}Sr$ is increased slightly and also Ba, Rb and K are taken up (Hart and Staudigel 1989) and this process could explain some of the chemi-

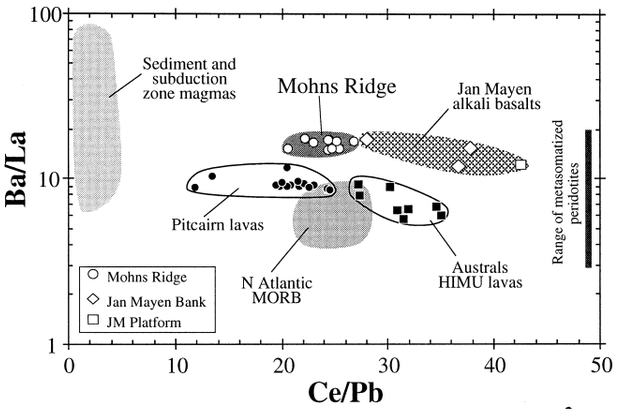

Fig. 11 Ba/La versus Ce/Pb for various lavas and reservoirs. N Atlantic MORB includes Ba, La, and Ce data for Kolbeinsey lavas from Devey et al. (1994) and Pb from Mertz et al. (1991). Other data from Ben Othman et al. (1989), Chauvel et al. (1992), Woodhead and Devey (1993) and Hartmann and Wedepohl (1990)

cal signatures of the Mohns Ridge samples. However, other incompatible elements in Mohns MORB have ratios which are typical for the oceanic mantle. Mohns MORB have "normal" oceanic Ce/Pb ratios ($\sim$25, Hofmann et al. 1986) while the Ce/Pb ratios of Jan Mayen alkali basalts appear to be higher (Fig. 11). Sediments have low Ce/Pb due to their high Pb contents, and a sediment component in the source would strongly change the Ce/Pb of the mantle (Hofmann et al. 1986). Also the Rb/Cs ratios of the Mohns tholeiites lie in the range of 80 ± 10 which is typical for oceanic lavas (Hofmann and White 1983) and thus contradict the model of recycled sediment in the northern Norwegian–Greenland Sea mantle. In Fig. 11 the Mohns lavas resemble neither the HIMU type lavas (probably generated from recycled oceanic crust, e.g. Chauvel et al. 1992) nor the Pitcairn lavas (thought to be generated from mantle enriched by recycled sediment, e.g. Woodhead and Devey 1993). As we had shown above the enrichments of Cs, Ba, Rb, and K compared to other incompatible elements are frequently found in subduction-related basalts and in metasomatized peridotites (Figs. 7 and 11) implying a fractionation of these elements from those of similar incompatibility (like La or Nb) during partial melting. If this fractionation is due to phlogopite (see 5.2) then this could also lead to a buffering of Ce/Pb in the alkali basalts (Fig. 11) as it appears to strongly incorporate Pb (Ionov and Hofmann 1995).

The cause of magmatism at Jan Mayen

Two models are generally proposed to explain the generation of geochemically enriched magmas such as those which occur near Jan Mayen. The first envisages an enriched plume ascending underneath the island which contributes to the magmas about 100 km south and 200 km north of the fracture zone but which also influences Knipovich Ridge (Neumann and Schilling 1984; Waggoner 1989). In the second model of small scale heterogeneous mantle melts sequentially by passive upwelling (Zindler et al. 1984; Sleep 1984). Volcanism at fracture zones has been observed in the Pacific and was explained by abundant faulting and fracture zone weakness (Lowrie et al. 1986). To choose between these possibilities we have to investigate whether there are physical signs of a plume in the area, and whether the enriched component can be mixed into the spreading centre magmas by a point-like influx from a plume from the lower parts of the mantle.

The most significant sign of a mantle plume from the deep mantle (>600 km depth) is the track of volcanoes it creates on the overriding lithosphere. Johnson and Campsie (1976) and Waggoner (1989) included Vesteris Seamount, Vøring Plateau and the Hold with Hope flood basalts in E Greenland into a Jan Mayen plume track. Vesteris Seamount was shown to be younger than 1 Ma (Mertz and Renne 1994) while the large volumes of lava of Vøring Plateau and Hold with Hope are probably derived from the influence of the Iceland plume (Vink 1984). For the time between 55 and 5 Ma no physical signs of plume volcanism have been found in the Norwegian–Greenland Sea (Vogt 1986). Schilling (1976) suggested ascending blobs of hot mantle generating discontinuous volcanism starting with the formation of the Vøring Plateau 55 Ma ago and leading to the Jan Mayen volcanism 50 Ma later. However, geophysical models predict excessive volcanism during the first phase of plume head impact under the lithosphere leading to oceanic plateau generation (Griffiths and Campbell 1990). This is not observed in the Jan Mayen region.

Neither is there evidence for a bathymetric anomaly. Although Schilling (1991) proposes a 2200 m positive bathymetric anomaly for the Jan Mayen area, this appears extreme, as Eggvin Bank and Jan Mayen Platform are, at least in part, fracture zone ridges (Menard and Atwater 1969; Bonneville and McNutt 1992) set onto the uplifted region of the Iceland Plateau. The water depth north of the 50 km long Jan Mayen Platform increases by 2 km, leading to globally normal depths of 2.5–3 km of the spreading axis only 100 km away from the WJMFZ on Mohns Ridge (Neumann and Schilling 1984). There is no bathymetric evidence for a plume swell.

Direct evidence against a heat anomaly underneath Jan Mayen comes from seismic investigations. There is only a weak attenuation of seismic waves beneath the area of the island as would be expected from a volcanically active centre near a fracture zone (Havskov et al. 1986). Seismic tomography shows no evidence for an unusually warm mantle beneath the Jan Mayen area (Zhang and Tanimoto 1993). Vogt (1986) and Havskov and Atakan (1991) noted that earthquake epicentres at the WJMFZ occur as deep as 40 km and thought this to be improbable in lithosphere heated above a plume.

The oceanic lithosphere around Jan Mayen is about 20 Ma years old, while opposite the island on the northern side of the WJMFZ the age of the crust is 0 to 5 Ma

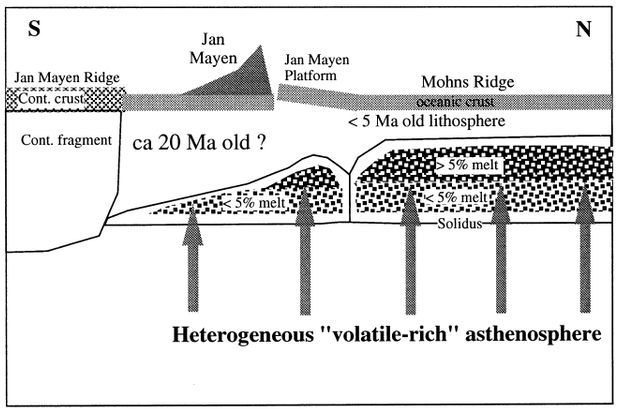

Fig. 12 Schematic drawing of the possible configuration of the melting zones underneath Mohns Ridge and Jan Mayen as implied by the petrological data. Compare with the geophysical models of Phipps Morgan and Forsyth (1988)

at the Jan Mayen Platform spreading axis. On the Jan Mayen Platform mainly alkali basalts occur, not what would be expected if anomalously hot mantle ascends to shallow depths in this axis. The Platform Ridge alkali basalts are probably generated by less than 5% melting in the garnet stability field (>60 km depth) (Neumann and Schilling 1984), thus melting beneath the Platform is apparently depressed to greater depths relative to normal ridge segments. An effect of lowering the mantle temperature was suggested to occur at fracture zones (Langmuir and Bender 1984; Fox and Gallo 1984). Model calculations of Phipps Morgan and Forsyth (1988) showed that within 25 km of a fracture zone at a spreading rate of 1 cm/a and 100 km offset, the upper mantle temperature is several hundred degrees C cooler than in the surrounding mantle. Our results from the WJMFZ area are in accordance with these models, as mainly alkaline lavas erupt in the vicinity of the fracture zone, suggesting a decreased degree of melting ("transform fault effect"of Langmuir and Bender 1984). Schilling and Sigurdsson (1979) have shown that lavas in the vicinity of the WJMFZ have eruption temperatures about 100° C lower than along the neighbouring spreading axes thus also supporting a low-temperature mantle near Jan Mayen. Evidence shown earlier for the effect of a hydrous phase on the lava chemistry implies that melting along the Platform Ridge may only be possible because water in the mantle lowers the solidus temperature sufficiently.

The upwelling of mantle material into the Platform Ridge axis may have a buoyancy effect across the fracture zone as the area of melt generation along spreading axes is much wider than the volcanic zone itself. Thus small volume melts may form underneath the island Jan Mayen. As the isotherms in the mantle lie at greater depths below the WJMFZ the magmas are low degree melts (alkali basalts). From the petrological considerations we can construct the zones of melting for the region north of Jan Mayen which resemble closely the geophysical model of Phipps Morgan and Forsyth (1988) (Fig. 12). The ascent of the magmas to the surface may be possible because the lithosphere underneath Jan Mayen is weakened due to its position between the continental fragment of the Jan Mayen Ridge (Skogseid and Eldholm 1987) and the fracture zone or by the fracture zone alone. Thus volcanism at Jan Mayen is the result of the unique coincidence of a continental fragment, a fracture zone and a spreading axis.

Concluding remarks

1. Lavas on the Mohns Ridge north of Jan Mayen have variable compositions with the majority of the lavas on the spreading axis being alkali basalts and enriched tholeiitic rocks. On a large scale there is a continuity of compositions between the lavas from the island Jan Mayen and the basalts from the spreading axis in incompatible element and isotopic composition. This suggests a heterogeneous mantle with low melting point, enriched heterogeneities which are preferentially melted into the small degree ($\sim$5%) melts near Jan Mayen and whose melts are more diluted further north at 72°N.
2. Three lava types with different incompatible element compositions, e.g. $(La/Sm)_N<1$ to >2, occur in the area at 72°N and were generated by mixing of large degree melts with small degree melts from more enriched parts of the mantle. The elements Ba, Rb and K of the small degree melt were probably buffered in the mantle by a residual phase like phlogopite or amphibole.
3. Mohns MORB and Jan Mayen area alkali basalts have high contents of Cs, Ba, Rb, and K compared to other incompatible elements (e.g. Ba/La of about 15). These ratios reflect the signature of the mantle source. The ratios Ce/Pb and Rb/Cs have normal mantle values of 25 and 80, respectively, thus the enrichments of Ba and Rb are not due to a sedimentary component. The source was probably generated by metasomatic input of Cs, Ba, Rb and K into the mantle. The fluid appears to resemble to some extent that released from a subducting slab.
4. Geophysical and petrological observations contradict the Jan Mayen plume model as there is no plume track and no geophysical or petrological/geochemical evidence for mantle with an excess temperature underneath Jan Mayen. It appears more likely that the melting is induced by passive upwelling of volatile-rich mantle due to the influence of the nearby spreading axis.

Acknowledgements We thank the captains and crew of FS Meteor and FS Polarstern for their help with the work on the ships. H. Lass is thanked for help with ICP-MS analyses and D. Ackermand and B. Mader for help with the microprobe. We appreciate comments by W. Bach on a first draft of this paper, and the official reviews by A. Brandon and an anonymous reviewer. K.M.H. gratefully acknowledges support by a grant from the Deutsche Forschungsgemeinschaft through the Graduiertenkolleg "Dynamik globaler Kreisläufe im System Erde". The research was funded by the Bundesministerium for Forschung und Technologie grants 03R601 7 and 03R615 7 to P. Stoffers.

References

Adam J, Green TH, Sie SH (1993) Proton microprobe determined partitioning of Rb, Sr, Ba, Y, Zr, Nb and Ta between experimentally produced amphiboles and silicate melts with variable F contents. Chem Geol 109: 29–49

Ahern JL, Turcotte DL (1978) Magma migration beneath an ocean ridge. Earth Planet Sci Lett 45: 115–122

Ballhaus C (1993) Redox states of lithospheric and asthenospheric upper mantle. Contrib Mineral Petrol 114: 331–348

Ben Othman D, White WM, Patchett J (1989) The geochemistry of marine sediments, island arc magma genesis, and crust-mantle recycling. Earth Planet Sci Lett 94: 1–21

Bonatti E, Ottonello G, Hamlyn PR (1986) Peridotites from the Island of Zabargad (St. John), Red Sea: petrology and geochemistry. J Geophys Res 91: 599–631

Bonneville A, McNutt M (1992) Shear strength of great Pacific fracture zones. Geophys Res Lett 19: 2023–2026

Bott MHP (1985) Plate tectonic evolution of the Icelandic transverse ridge and adjacent regions. J Geophys Res 90: 9953–9960

Bougault H, Dimitriev L, Schilling J-G, Sobolev A, Joron J-L, Needham HD (1988) Mantle heterogeneity from trace elements: MAR triple junction near 14°N. Earth Planet Sci Lett 88: 27–36

Castillo P, Batiza R (1989) Strontium, neodymium and lead isotope constraints on near-ridge seamount production beneath the South Atlantic. Nature 342: 262–265

Chauvel C, Hofmann AW, Vidal P (1992) HIMU-EM: the French Polynesian connection. Earth Planet Sci Lett 110: 99–119

Dauteuil O, Brun J-P (1993) Oblique rifting in a slow-spreading ridge. Nature 361: 145–148

Devey CW, Garbe-Schönberg C-D, Stoffers P, Chauvel C, Mertz DF (1994) Geochemical effects of dynamic melting beneath ridges: reconciling major and trace elements variations in Kolbeinsey (and global) MORB. J Geophys Res 99: 9077–9095

Dosso L, Hanan BB, Bougault H, Schilling J-G, Joron J-L (1991) Sr-Nd-Pb geochemical morphology between 10 and 17°N on the Mid-Atlantic Ridge: a new MORB isotope signature. Earth Planet Sci Lett 106: 29–43

Fox PJ, Gallo DG (1984) A tectonic model for ridge-transform-ridge plate boundaries: implications for the structure of oceanic lithosphere. Tectonophysics 104: 205–242

Galer SJG, O'Nions RK (1986) Magmagenesis and the mapping of chemical and isotopic variations in the mantle. Chem Geol 56: 45–61

Garbe-Schönberg CD (1993) Simultaneous determination of thirty-seven trace elements in twenty-eight international rock standards by ICP-MS. Geostand Newsl 17: 81–97

Géli L (1993) Volcano-tectonic events and sedimentation since Late Miocene times at the Mohns Ridge, near 72°N, in the Norwegian–Greenland Sea. Tectonophysics 222: 417–444

Govindaraju K (1994) 1994 compilation of working values and sample-description for 383 geostandards. Geostand Newsl 18

Green TH (1994) Experimental studies of trace-element partitioning applicable to igneous petrogenesis – Sedona 16 years later. Chem Geol 117: 1–36

Griffiths RW, Campbell IH (1990) Stirring and structure in mantle starting plumes. Earth Planet Sci Lett 99: 66–78

Gudfinnsson GH, Presnall DC (1993) Phase compositions along the model lherzolite solidus in the system CaO-MgO-Al_2O_3-SiO_2 from 20 to 34 kbar. Eos Trans Am Geophys Union 74: 658

Haase KM, Devey CW (1994) The petrology and geochemistry of Vesteris Seamount, Greenland Basin – an intraplate alkaline volcano of non-plume origin. J Petrol 35: 295–328

Hart SR, Staudigel H (1989) Isotopic characterization and identification of recycled components. In: Hart SR, Gülen L (eds) Crust/mantle recycling at convergence zones. Kluwer Academic Press, Amsterdam, pp 15–28

Hartmann G, Wedepohl KH (1990) Metasomatically altered peridotite xenoliths from the Hessian Depression (Northwest Germany). Geochim Cosmochim Acta 54: 71–86

Havskov J, Atakan K (1991) Seismicity and volcanism of Jan Mayen Island. Terra Nova 3: 517–526

Havskov J, Kvamme LB, Bungum H (1986) Attenuation of seismic waves in the Jan Mayen Island area. Mar Geophys Res 8: 39–47

Hawkesworth CJ, Gallagher K, Hergt JM, McDermott F (1993) Mantle and slab contributions in arc magmas. Annu Rev Earth Planet Sci 21: 175–204

Hergt JM, Farley KN (1994) Major element, trace element, and isotope (Pb, Sr, and Nd) variations in site 834 basalts: implications for the initiation of backarc opening. In: Hawkins J, Parson L, Allan J et al. Proc ODP Sci Results 135: 471–486

Hirose K, Kawamoto T (1995) Hydrous partial melting of lherzolite at 1 GPa: the effect of H_2O on the genesis of basaltic magmas. Earth Planet Sci Lett 133: 463–473

Hofmann AW (1988) Chemical differentiation of the Earth: the relationship between mantle, continental crust, and oceanic crust. Earth Planet Sci Lett 90: 297–314

Hofmann AW, White WM (1983) Ba, Rb and Cs in the Earth's mantle. Z Naturforsch 38a: 256–266

Hofmann AW, Jochum KP, Seufert M, White WM (1986) Nb and Pb in oceanic basalts: new constraints on mantle evolution. Earth Planet Sci Lett 79: 33–45

Imsland P (1980) The petrology of the volcanic island Jan Mayen, Arctic Ocean. Nord Volcanol Inst Iceland Internal Rep 8003

Ionov DA, Hofmann AW (1995) Nb-Ta-rich mantle amphiboles and micas: implications for subduction-related metasomatic trace element fractionations. Earth Planet Sci Lett 131: 341–356

Jochum K-P, Seufert HM, Thirlwall MF (1990) Multi-element analysis of 15 international standard rocks by isotope-dilution spark source mass spectrometry. Geostand Newsl 14: 469–473

Johnson GL, Campsie J (1976) Morphology and structure of the Western Jan Mayen Fracture Zone. Nor Polarinst Arbok 1974: 69–81

Kinzler RJ, Grove TL (1992) Primary magmas of mid-ocean ridge basalts. 2. Applications. J Geophys Res 97: 6907–6926

Klein EM, Langmuir CH (1987) Global correlations of ocean ridge basalt chemistry with axial depth and crustal thickness. J Geophys Res 92: 8089–8115

Kurz MD, Jenkins WJ, Hart SR (1982) Helium isotopic systematics of oceanic islands and mantle heterogeneity. Nature 297: 43–46

Langmuir CH, Bender JF (1984) The geochemistry of oceanic basalts in the vicinity of transform faults: observations and implications. Earth Planet Sci Lett 69: 107–127

Lowrie A, Smoot C, Batiza R (1986) Are oceanic fracture zones locked and strong or weak?: new evidence for volcanic activity and weakness. Geology 14: 242–245

Maaløe S, Sørensen IB, Hertogen J (1986) The trachybasaltic suite of Jan Mayen. J Petrol 27: 439–466

McKenzie D, O'Nions RK (1991) Partial melt distributions from inversion of rare earth element concentrations. J Petrol 32: 1021–1091

Menard HW, Atwater T (1969) Origin of fracture zone topography. Nature 222: 1037–1040

Mengel K, Green DH (1989) Stability of amphibole and phlogopite in metasomatized peridotite under water-saturated and water-undersaturated conditions. In: Proc 4th Int Kimberlite Conf. Geol Soc Aust Spec Publ 14, pp 571–581

Mertz DF, Renne PR (1994) Quaternary multi-stage alkaline volcanism at Vesteris Seamount (Norwegian–Greenland Sea): evidence from laser step heating $^{40}Ar/^{39}Ar$ experiments. J Geodyn 19: 79–95

Mertz DF, Devey CW, Todt W, Stoffers P, Hofmann AW (1991) Sr-Nd-Pb isotope evidence against plume-asthenosphere mixing north of Iceland. Earth Planet Sci Lett 107: 243–255

Michael PJ, Chase RL (1987) The influence of primary magma composition, H_2O and pressure on mid-ocean ridge basalt differentiation. Contrib Mineral Petrol 96: 245–263

Morgan WJ (1981) Hotspot tracks and the opening of the Atlantic and Indian Oceans. In: Emiliani C (ed) The oceanic lithosphere. (The sea, vol 7) Wiley and Sons, New York, pp 443–487
Myhre AM, Eldholm O, Sundvor E (1984) The Jan Mayen Ridge: present status. Polar Res 2: 47–59
Neubourg B (1990) Systematische Untersuchungen zu Aufschlußverfahren basaltischen Materials für ICP-MS-Messungen (unpublished) Dipl thesis Univ Kiel
Neumann E-R, Schilling J-G (1984) Petrology of basalts from the Mohns-Knipovich Ridge; the Norwegian–Greenland Sea. Contrib Mineral Petrol 85: 209–223
Nunns A (1982) The structure and evolution of the Jan Mayen Ridge and surrounding regions. Am Assoc Petrol Geol Mem 34: 193–208
O'Nions RK, Pankhurst RJ (1974) Petrogenetic significance of isotope and trace element variations in volcanic rocks from the Mid-Atlantic. J Petrol 15: 603–634
Parsons PB, Sclater JG (1977) An analysis of the variation of ocean floor bathymetry and heat flow with age. J Geophys Res 82: 803–827
Perry RK (1986) Bathymetry. In: Hurdle BG (ed) The Nordic Seas. Springer, Berlin Heidelberg New York, pp 211–233
Phipps Morgan J (1987) Melt migration beneath mid-ocean spreading centers. Geophys Res Lett 14: 1238–1241
Phipps Morgan J, Forsyth DW (1988) Three-dimensional flow and temperature perturbations due to a transform offset: effects on oceanic crustal and upper mantle structure. J Geophys Res 93: 2955–2966
Plank T, Langmuir CH (1992) Effects of the melting regime on the composition of the oceanic crust. J Geophys Res 97: 19749–19770
Saemundsson K (1986) Subaerial volcanism in the western North Atlantic. In: Vogt PR, Tucholke BE (eds) The geology of North America. Vol M. The western North Atlantic region. Geol Soc Am, Boulder, Colorado, pp 69–86
Savostin LA, Karasik AM (1981) Recent plate tectonics of the Arctic Basin and of northeastern Asia. Tectonophysics 74: 111–145
Schilling J-G (1976) Rare-earth, Sc, Cr, Fe, Co, and Na abundances in DSDP Leg 38 basement basalts: some additional evidence on the evolution of the Thulean Province. Initial Rep DSDP 38: 741–750
Schilling J-G (1991) Fluxes and excess temperatures of mantle plumes inferred from their interaction with migrating mid-ocean ridges. Nature 352: 397–403
Schilling J-G, Sigurdsson H (1979) Thermal minima along the axis of the Mid-Atlantic Ridge. Nature 282: 370–375
Schilling J-G, Bergeron MB, Evans R (1980) Halogens in the mantle beneath the North Atlantic. Philos Trans R Soc London A297: 147–178
Schilling J-G, Zajac M, Evans R, Johnston T, White W, Devine JD, Kingsley R (1983) Petrologic and geochemical variations along the Mid-Atlantic Ridge from 29°N to 73°N. Am J Sci 283: 510–586
Shaw DM (1970) Trace element fractionation during anatexis. Geochim Cosmochim Acta 34: 237–243
Shirey SB, Bender JF, Langmuir CH (1987) Three-component isotopic heterogeneity near the Oceanographer transform, Mid-Atlantic Ridge. Nature 325: 217–223
Sigurdsson H (1981) First-order major element variation in basalt glasses from the Mid-Atlantic Ridge: 29°N to 73°N. J Geophys Res 86: 9483–9502
Skogseid J, Eldholm O (1987) Early Cenozoic crust at the Norwegian continental margin and the conjugate Jan Mayen Ridge. J Geophys Res 92: 11471–11491
Sleep NH (1984) Tapping of magmas from ubiquitous mantle heterogeneities: an alternative to mantle plumes? J Geophys Res 89: 10029–10041
Sleep NH (1990) Hotspots and mantle plumes: some phenomenology. J Geophys Res 95: 6715–6736
Sudo A, Tatsumi Y (1990) Phlogopite and K-amphibole in the upper mantle: implication for magma genesis in subduction zones. Geophys Res Lett 17: 29–32
Sun SS, McDonough WF (1989) Chemical and isotope systematics of oceanic basalts: implications for mantle composition and processes. In: Saunders AD, Norry MJ (eds) Magmatism in the ocean basins. Geol Soc Spec Publ 42, pp 313–345
Sylvester AG (1975) History and surveillance of volcanic activity on Jan Mayen Island. Bull Volcanol 39: 1–23
Tatsumi Y, Hamilton DL, Nesbitt AW (1986) Chemical characteristics of the fluid phase released from the subducted lithosphere and origin of arc magmas: evidence from high pressure experiments and natural rocks. J Volcanol Geothermal Res 29: 293–309
Vink GE (1984) A hotspot model for Iceland and the Vøring Plateau. J Geophys Res 89: 9949–9959
Vogt PR (1986) Geophysical and geochemical signatures and plate tectonics. In: Hurdle BG (ed) The Nordic Seas. Springer, Berlin Heidelberg New York, pp 413–662
Waggoner DG (1989) An isotopic and trace element study of mantle heterogeneity beneath the Norwegian–Greenland Sea (unpublished). PhD thesis, Univ of Rhode Island, USA
Woodhead JD (1989) Geochemistry of the Mariana arc (western Pacific): source composition and processes. Chem Geol 76: 1–24
Woodhead JD, Devey CW (1993) Geochemistry of the Pitcairn seamounts. I. Source character and temporal trends. Earth Planet Sci Lett 116: 81–99
Zhang Y-S, Tanimoto T (1993) High-resolution global upper mantle structure and plate tectonics. J Geophys Res 98: 9793–9823
Zindler A, Staudigel H, Batiza R (1984) Isotope and trace element geochemistry of young Pacific seamounts: implications for the scale of upper mantle heterogeneity. Earth Planet Sci Lett 70: 175–195